FREQUENCY-DOMAIN METHODOLOGY FOR PRACTICAL GROUND RESONANCE ANALYSIS AND TEST

Richard L. Bielawa

R. L. Bielawa Associates, Inc.
Sequim, WA USA

Abstract

A new method for analyzing helicopter ground resonance is presented that rectifies two important deficiencies that traditional eigenvalue-based methodologies can only address approximately: the presence of system nonlinearities and the practical use of vibration test data for analysis validation. This new methodology is based on frequency-domain characterizations of both the rotor and fuselage components of the problem. Additionally, this new methodology enables the analysis of the doubly anisotropic problem of one dissimilar lead-lag damper (either inoperative or with reduced effectiveness) without recourse to Floquet theory. Results are presented showing the utility and effectiveness of the methodology.

Nomenclature

C_b = blade lead-lag damping rate, lb-ft-s

C_{xF}, C_{yF} = damping coefficients for fuselage (hub) in longitudinal and lateral directions, respectively, lb-s/ft

c = blade chord, ft

e = radial offset distance of lead-lag hinge, ft

FRF = frequency response function

$\boldsymbol{G}_1$ = mobility matrix of fuselage (with included rotor mass)

$\boldsymbol{G}_2$ = impedance matrix for the rotor lead-lag motion

H = hub distance above the pivot point, ft

$\boldsymbol{H}_{11}$ = impedance matrix of fuselage (with included rotor mass)

$\boldsymbol{H}_{12}$, $\boldsymbol{H}_{21}$ = rotor to fuselage and fuselage to rotor coupling matrices, respectively

$\boldsymbol{H}_{22}$ = impedance matrix of rotor lead-lag motion

I_b = second mass moment of inertia of rotor blade about lead-lag hinge, lb-ft-s^2

K_e = blade lead-lag damper effectivity factor

K_{xF}, K_{yF} = effective hub stiffness in the longitudinal and lateral directions, respectively, lb/ft

M_{DF} = nonlinear dry friction damping moment coefficient, lb-in

M_{HD} = nonlinear hydraulic damping moment coefficient, lb-in-s^2

m_b = mass of rotor blade, lb-s^2/ft

n = number of blades

R = rotor blade radius, ft

S_b = first mass moment of rotor blade about the lead-lag hinge, lb-s^2

t = time, s

$\boldsymbol{X}_F$ = state vector of fuselage (hub) variables

$\boldsymbol{X}_R$ = state vector of rotor lead-lag response variables

x, y = longitudinal and lateral deflections, respectively, of the rotor hub

θ = pitching deflection of fuselage/shaft mass about the base pivot point, (= x/H), rad

Λ = characteristic multiplier

$\Lambda_{EQUIV(\alpha)}$ = equivalent characteristic multiplier of conventional eigenvalue, for comparison with Λ, [=exp($\alpha\sigma$)]

λ = eigenvalue, (= $\sigma \pm i\omega$), s^{-1}

λ_{GR} = eigenvalue corresponding to the ground resonance instability, s^{-1}

ε_x, ε_y = blade lead-lag multi-blade coordinates in the longitudinal and lateral directions, respectively, rad

η_i = blade damping coefficient for the ith blade group, [= $(C_b/I_b)_i$], s

σ = real part of the eigenvalue, s^{-1}

σ_{EFF} = effective (approximate) real part of eigenvalue of a characteristic multiplier for comparison with σ, s^{-1}

ω = alternatively, scan frequency and imaginary part of the eigenvalue, rad/s

ω_e = blade lead-lag natural frequency at rotor speed, [= $\Omega\,(eS_b/I_b)^{1/2}$], rad/s

Ω = rotor speed, alternatively, rad/s and RPM

$(\ldots)^*$ = for conditions when a characteristic multiplier crosses the real axis

$(\ldots)^{(i)}$ = index on blade group, i = (1, opposing undifferentiated blades, 2, the one dissimilar blade, 3, remaining undifferentiated blade opposing the differentiated blade)

Presented at the 28th European Rotorcraft Forum, Bristol, UK, September 17-20, 2002

Introduction

With the increased attention to operational requirements, the assurance of ground resonance stability in the operational envelope requires increasing attention to nonlinearities. Several traditional sources of nonlinearities continue to require attention. Hydraulic lead-lag dampers do not give forces exactly proportional to velocity and typically have significant saturation characteristics. Likewise, landing gear oleo dampers have significant nonlinear characteristics, including hysteretic breakout forces. Tires, an important source of damping, likewise have nonlinear characteristics. Even with skid landing gears, the presence of friction as a source of landing gear damping, defines a classic form of nonlinearity. However, even apart from these usual sources of nonlinearities, there are increasing operational requirements imposed on modern helicopters that define significant nonlinear processes (landing skid friction on a variety of set-down surfaces, the presence of specialized restraining mechanisms, etc.)

Apart from the consideration of nonlinearities is the ever-present chore of validating the analytic ground resonance model with experimental test data to characterize the fuselage dynamics. As with any analytic prediction, validation of ground resonance calculations with test data is always in order. The problem here is that the usual data required for all eigenvalue-based analyses is the identification and evaluation of the *separate* equivalent (linearized) parameters, i.e., masses, stiffnesses and damping levels for each of the various modes. The characterization of these parameters with test data is confounded by the fact that modern vibration testing is done in the *frequency domain.* Indeed, much effort has been expended in producing test equipment and data processing algorithms capable of measuring, with a high degree of accuracy, frequency response functions, *FRF's* (consisting of frequency dependent amplitudes and phase angles) for selected ranges of frequencies. Thus, the subsequent evaluations of the required equivalent masses, stiffnesses and damping levels must be made judiciously from frequency-domain data. This process invariably requires ingenuity, needlessly introduces additional sources of error, and is required only because of the data requirements of an eigenvalue analysis.

The new frequency-domain based methodology presented herein corrects these deficiencies. It requires the separate use of frequency dependent "rotor impedance" and "fuselage mobility" characteristics. "Fuselage mobility" is essentially a multi-variant form of a frequency response function that can be either calculated and/or measured directly. Calculation of the fuselage mobility is a straightforward process when the dynamic description of the fuselage is linear. When significant nonlinearities occur, numerical integration of the nonlinear equations of motion must be used to obtain these dynamic characteristics, since all conceivable nonlinearities can be modeled in the time-domain. Hence, frequency response functions, as obtained either analytically or experimentally, can be *directly* applied to the ground resonance evaluation with maximum accuracy. The rotor subsystem is usually quite linear except for the presence of nonlinearities in the lead-lag dampers. Even for this case, however, the required dynamic characteristics can again be obtained using numerical integration of the appropriate equations of motion.

Description of the Methodology

Basic Mathematical Idea

The new methodology is a multi-variant form of the classic Nyquist stability criterion, a well-established element of control system technology for single degree-of-freedom dynamics (Ref 1, e.g.). The new methodology, as originally outlined by the author 18 years ago in a different context (see Ref 2), expands on the Nyquist criterion idea, to include multiple degree-of-freedom dynamics. The basic idea is to partition the dynamic problem into two distinct and interacting subsystems:

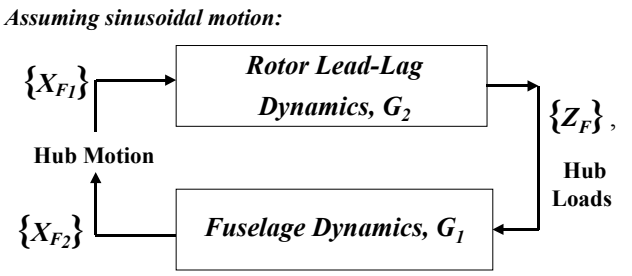

Fig. 1 Conceptualization of the rotor-airframe interaction

For purposes herein we define $\boldsymbol{G_1}$ to be the pylon (i.e., fuselage) mobility, (displacement per force) and $\boldsymbol{G_2}$ to be the rotor impedance, (i.e., force per displacement), both of which are at the same time matrix quantities and functions of frequency, ω. The crux of the method is to reconnect these subsystems with the introduction of a set of ***characteristic multipliers***, $\Lambda(\omega)$, thereby forming a new matrix eigenvalue problem. Since both $\boldsymbol{G_1}$ and $\boldsymbol{G_2}$ are functions of frequency, so too, the characteristic multipliers will also be frequency dependent:

$$[G_1(\omega)][G_2(\omega)]\{X\} = \Lambda(\omega)\{X\} \tag{1}$$

The eigenvalues of this equation, $\Lambda(\omega)$, (i.e., the characteristic multipliers), are then easily determined

by conventional matrix eigenvalue methods. The variations of the eigenvalues commensurate with an arbitrarily selected variation in frequency define loci in the complex plane. ***Instability or stability is determined, respectively, by whether or not any of these loci encloses the point 1 + i0 in the complex plane***. Experience has shown that the frequency variation need only be performed in the frequency range where ground resonance instability would be an issue. Fig. 2 depicts this criterion and contrasts it with the usual eigenvalue stability criterion.

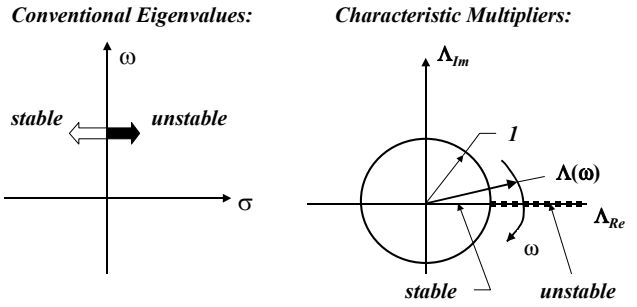

Fig. 2 Comparison of stability criteria

Application to the Ground Resonance Problem

The [$\boldsymbol{G_1} \bullet \boldsymbol{G_2}$] matrix product required for the ground resonance problem is obtained from the basic equations of motion (e.g., Refs 3,4). For sinusoidal motion the equations governing the fuselage hub & rotor mass displacements and rotor lead-lag degree-of-freedom variables, $\boldsymbol{X_F} = \boldsymbol{X}_{FUSELAGE+ROTOR\ MASS}$ & $\boldsymbol{X_R} = \boldsymbol{X}_{LEAD\text{-}LAG\ MOTION}$, can be expressed as:

$$\left[\begin{array}{c|c} H_{11}(\omega) & H_{12}(\omega) \\ \hline H_{21}(\omega) & H_{22}(\omega) \end{array}\right]\left\{\begin{array}{c} X_F \\ \hline X_R \end{array}\right\} = \{0\} \qquad (2)$$

The $\boldsymbol{H_{11}}$ and $\boldsymbol{H_{22}}$ matrices represent the uncoupled fuselage hub (plus rotor mass) and rotor lead-lag mode dynamics, respectively. The $\boldsymbol{H_{22}}$ matrix consists of the usual terms, as identified in the ground resonance literature. The $\boldsymbol{H_{12}}$ and $\boldsymbol{H_{21}}$ matrices are those involving simple mass-related coupling, also as identified in the literature. The requisite [$\boldsymbol{G_1} \bullet \boldsymbol{G_2}$] matrix product is then formed from the $\boldsymbol{H_{11}}$, $\boldsymbol{H_{12}}$, $\boldsymbol{H_{21}}$ and $\boldsymbol{H_{22}}$ matrices. Eq. 2 can be rewritten as two equations representing respectively the fuselage dynamics with rotor excitation and the rotor lead-lag motion dynamics with fuselage excitation:

$$[H_{11}]\{X_F\} = -[H_{12}]\{X_R\} \qquad (3a)$$

$$[H_{22}]\{X_R\} = -[H_{21}]\{X_F\} \qquad (3b)$$

The component vectors are then isolated:

$$\{X_F\} = -[H_{11}]^{-1}[H_{12}]\{X_R\} \qquad (4a)$$

$$\{X_R\} = -[H_{22}]^{-1}[H_{21}]\{X_F\} \qquad (4b)$$

and related to each other as a matrix eigenvalue problem:

$$\Lambda(\omega)\{X_F\} = [H_{11}]^{-1}[H_{12}][H_{22}]^{-1}[H_{21}]\{X_F\} \qquad (5)$$

where:

$$[G_1] = [H_{11}]^{-1} \qquad (6a)$$

$$[G_2] = [H_{12}][H_{22}]^{-1}[H_{21}] \qquad (6b)$$

Note that the methodology works equally well when:

$$[G_1] = [H_{22}]^{-1} \qquad (7a)$$

$$[G_2] = [H_{21}][H_{11}]^{-1}[H_{12}] \qquad (7b)$$

The choice of decomposition (i.e., using Eqs. 6a,b or 7a,b) is arbitrary, but some computation time would be saved by using the resulting smaller-sized [$\boldsymbol{G_1} \bullet \boldsymbol{G_2}$] matrix. For instance, if the fuselage dynamics involved a full complement of degrees of freedom of six, then Eqs. 7a&b would be preferable since the size of the $[H_{22}]^{-1}$ matrix is generally only 2×2, whereas the $[H_{11}]^{-1}$ matrix would be 6×6.

Analytically, either $\boldsymbol{G_1}$ and/or $\boldsymbol{G_2}$ can be calculated using a straightforward numerical integration of the nonlinear fuselage (or rotor) equations of motion. A standard high performance Runge-Kutta method (fourth order with Gill coefficients is typically used, see Ref 5), and then the time histories are Fourier analyzed for their fundamental harmonic cosine and sine components. [Note that these calculated quantities are the exact dynamic quantities that would be directly measured in subsequent ground vibration tests!] One practicality of this methodology is that, although either $\boldsymbol{G_1}$ and/or $\boldsymbol{G_2}$, can always be calculated in the time domain, for many conditions $\boldsymbol{G_2}$, the rotor impedance, is defined by linear terms. The required matrix inversion can then be performed quite simply and accurately without the integration of the equations of motion. The fuselage mobility requires the calculation of the matrix, $[H_{11}]^{-1}$, which actually constitutes *identically* the fuselage x- and y- direction sinusoidal responses due to sinusoidal (test) forces at the hub in the x- and y- directions i.e., *FRF*'s, (*frequency response functions*). For weakly nonlinear systems the choice of amplitude for the sinusoidal test forces would be of some concern. It would be prudent to keep the

amplitude small enough to maintain linearity and yet large enough to keep the results out of the "round-off noise".

The issue of the presence of nonlinearities in the system is implicitly addressed in this methodology, in that the fuselage mobilities thus calculated are "linear-effective" mobilities. (Note that these would consequently vary with response amplitude for nonlinear systems). While this procedure forms a "neat" way of addressing the nonlinearities, it needs to be stated that this form of linearization is no less valid than (and is actually equivalent to) the use of "describing functions" which are routinely used as a standard basis for linearization (e.g. Ref 6). Furthermore, as is presented later, the new methodology easily enables the prediction of limit cycle conditions resulting from nonlinearities. The analysis of limit cycle conditions requires that suitable variation of the sinusoidal test loads be made. Lastly, although not a nonlinearity per se, the condition of a failed or partially failed lead-lag damper (the doubly anisotropic problem) is also addressable by this methodology without recourse to Floquet theory.

Practical Implementation Issues

As formulated above, the basic equation, Eq. 1, is a matrix eigenvalue equation whose solution yields discrete values of the characteristic multipliers, Λ_j, as functions of discrete values of the scan frequency, ω_j. The search for the point of crossing of the real axis (in order to assess stability) must then be accomplished using supplementary techniques. First off, a suitable range of scan frequencies must be established. A convenient method is to identify a median frequency, ω_M, and then define the scan range using selected frequencies below and above that frequency. For the ground resonance problem the appropriate median frequency would be the "center of instability" frequency, defined by the slower blade progressive mode (i.e., the degenerate regressive mode after the rotor has gone supercritical). This frequency, as is well identified in the literature, is then given by:

$$\omega_M = \Omega - \omega_e \tag{8}$$

where ω_e is the blade lead-lag natural frequency (at rotor speed). It is then a straightforward programming exercise to evaluate the phases (or alternatively, the imaginary parts) of the characteristic multipliers to identify the real-axis crossing value. Specifically, a point in the frequency scan can be detected (*JJ*) wherein two consecutive values of the test quantity, $Im(\Lambda_j)$, are negative (i.e., $Im\ (\Lambda_j) < 0$, for $j = JJ,\ JJ - 1$) and the next two values are consecutively positive (i.e., $Im(\Lambda_j) > 0,\ j = JJ + 1,\ JJ + 2$). The use of cubic spline interpolation (Ref. 11) enables reasonably accurate interpolations of the function and its first derivative to be calculated, thereby enabling the use of a Newton-Raphson solution for calculating the value of frequency and characteristic multiplier at the point of zero phase, $\omega = \omega^*$ and $\Lambda = \Lambda(\omega^*)$, respectively.

The use of cubic spline fit interpolation also enables the (approximate) calculation of the second derivative of $\Lambda(\omega)$ at ω^*. As described in Appendix A, the first and second derivatives can be used to calculate effective modal stability exponents, σ_{EFF}, using analytic continuation. One post-processing chore that is recommended is to evaluate the maximum amplitude of each of the characteristic multipliers in the scan frequency range to verify that a possible significant characteristic multiplier doesn't get missed. The interested reader can devise any variety of post-processing operations with the characteristic multipliers to make the methodology most efficient for the purposes at hand.

Consistency of Eigenvalue Results with Characteristic Multiplier Results

The two basic methods for determining stability (i.e., linear eigenvalue vs. characteristic multiplier) use the basic matrix eigenvalue solution in distinctly different ways. In an attempt to show mathematical consistency between the two methods, they were separately used on *exactly* the same (linear) ground resonance equations of motion for a selected typical application. [It should be pointed out that the use of the characteristic multiplier approach is not restricted to either linear or nonlinear equation sets.] To this end the linear lead-lag damper value for a selected ground resonance configuration was artificially adjusted to produce three conditions: stable, exactly neutrally stable, and unstable. The results of this exercise are shown in Figs. 3a, 3b and 3c, respectively:

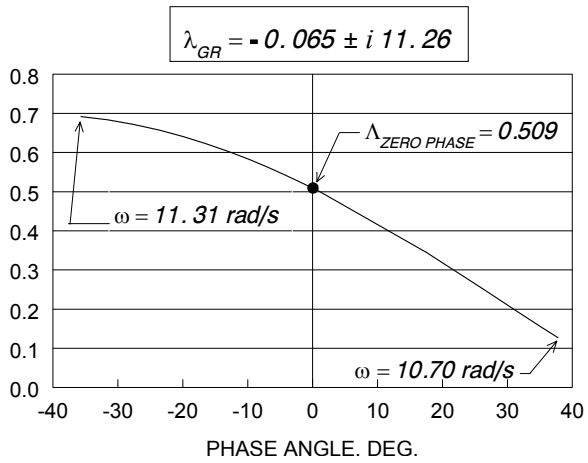

Fig 3a ~ stable case

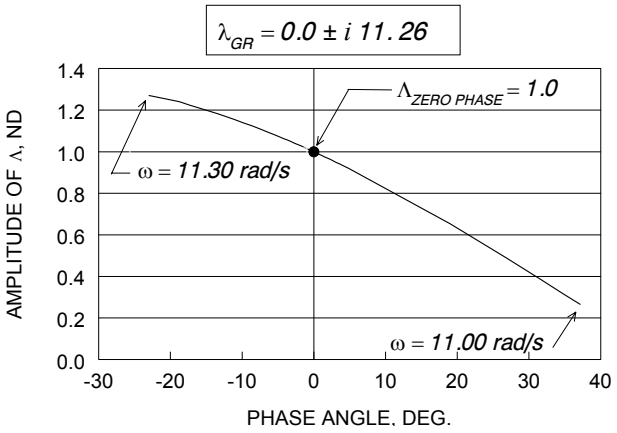

Fig 3b ~ neutrally stable case

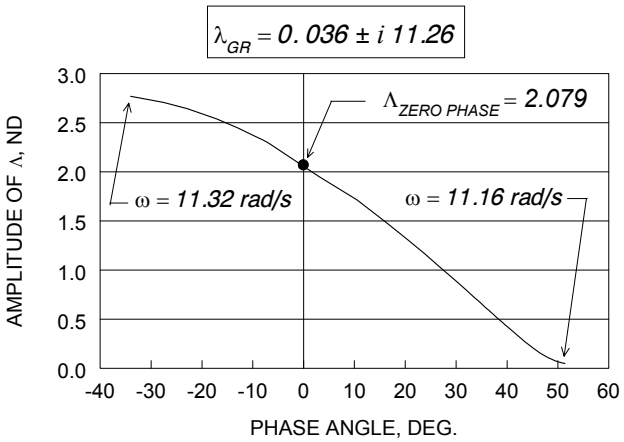

Fig. 3c ~ unstable case

Fig. 3 Characteristic multiplier vs. phase angle (representative results for linear systems)

These figures show the parametric variations of the respective characteristic multiplier magnitudes and phase angles with scan frequency, ω. Included in each of these figures are the values of the stability critical eigenvalues, as separately determined by the conventional eigenvalue solution. The figures clearly show that the methods do, indeed, give consistent qualitative indications of the stability of the system.

Quantitative Stability Characteristics

The principal utility of the characteristic multiplier approach is that it (numerically) gives qualitative stability vs. instability indications (i.e., the characteristic multiplier is either less than or greater than 1., as the system is stable or unstable). For even reasonably "small" systems, the method cannot *directly* give stability boundary information. This situation is similar to the stability boundary information afforded by the Routh-Hurwitz criterion for linear systems: For relatively small systems, the criterion can be used to formulate an *analytic* expression for the stability boundary, but otherwise it likewise gives just stability vs. instability information. Usually this information is sufficient for engineering purposes, however.

Now for some cases of instability it might be desirable to know quantitatively how much stability margin might be available. The conventional way to quantify this is to calculate the time to double amplitude from the modal damping exponent (as defined for linear systems). It can be safely assumed that the relative magnitude of the characteristic multiplier as it crosses the positive real axis is in some way an indicator of the relative stability (i.e., a small magnitude would indicate more stability than one close to unity). Thus, there is motivation to define an effective modal damping exponent from the characteristic multipliers. Such information would also serve to bridge the understanding of how results from the two methods (conventional eigenvalue analysis and frequency-domain analysis using characteristic multipliers) relate to each other. To this end formulations have been developed to approximate an "effective" modal damping exponent for each of the characteristic multipliers found using the frequency domain methodology. These formulations are provided in Appendix A.

The Dissimilar Lead-Lag Damper Problem

The frequency-domain methodology can also be extended to the case of dissimilar blades, as would be the case with a failed or partially failed lead-lag damper. A brief description of the extension of the basic methodology to this case is presented herein, while the details are presented in Appendix B. In order to retain the methodology in a form that still uses non-rotating coordinates, and especially the use of multi-blade coordinates, i.e., ε_x and ε_y, the following requirements must be met:

1. The rotor description must include the use of separate rotor mode coordinates (i.e., ε_x and ε_y pairs) for:
   a) the one blade with the dissimilar characteristics,
   b) the one blade opposite it, and
   c) the remaining blades that each have a matched blade opposite it.

As developed so (for only the four-bladed case), it would appear, by inference, that the methodology would require six multi-blade coordinates for rotors with an even number of blades and four for rotors with an odd number of blades.

2. The presence of the anisotropy in the rotor means that hub motions of frequency, ω, will produce excitations in the rotor of ω, $(2\Omega + \omega)$ and $(2\Omega - \omega)$, all of which can couple with the dynamics of the fuselage. Thus, in obtaining the appropriate fuselage hub *FRF*'s, in addition to sweeps in frequency ω, additional frequency sweeps must be obtained for the additional frequencies, as well. This requires that both the fuselage- and rotor-related state vectors contain components with each of these three frequencies:

$$\{X_F\} = \begin{Bmatrix} X_F^{(0)} e^{i\omega t} \\ X_F^{(I)} e^{i(\omega+2\Omega)t} \\ X_F^{(II)} e^{i(\omega-2\Omega)t} \end{Bmatrix} \tag{9a}$$

$$\{X_R\} = \begin{Bmatrix} X_R^{(0)} e^{i\omega t} \\ X_R^{(I)} e^{i(\omega+2\Omega)t} \\ X_R^{(II)} e^{i(\omega-2\Omega)t} \end{Bmatrix} \tag{9b}$$

3. Using the formulation defined by Eqs. 3a&b, the $\boldsymbol{G_1}$ and $\boldsymbol{G_2}$ matrices are then expressible as:

$$G_1(\omega) = H_{11}^{-1}(\omega) \tag{10a}$$

$$\begin{aligned} G_2(\omega) &= \left[H_{12}^{(0)}(\omega) + e^{2\Omega i} H_{12}^{(I)}(\omega) + e^{-2\Omega i} H_{12}^{(II)}(\omega)\right] \cdot \\ &\qquad \left[H_{22}(\omega)\right]^{-1}\left[H_{21}(\omega)\right] \\ &= G_2^{(0)}(\omega) + e^{2\Omega i} G_2^{(I)}(\omega) + e^{-2\Omega i} G_2^{(II)}(\omega) \end{aligned} \tag{10b}$$

The resulting eigenvalue equation relating $\boldsymbol{X_F}$ and $\boldsymbol{X_R}$ then becomes:

$$\Lambda\{X_F\} = \left[\begin{array}{c|c|c} G_1 G_2^{(0)}(\omega - 2\Omega) & G_1 G_2^{(II)}(\omega) & 0 \\ \hline G_1 G_2^{(I)}(\omega - 2\Omega) & G_1 G_2^{(0)}(\omega) & G_1 G_2^{(II)}(\omega + 2\Omega) \\ \hline 0 & G_1 G_2^{(I)}(\omega) & G_1 G_2^{(0)}(\omega + 2\Omega) \end{array}\right] \{X_F\} \tag{11}$$

Within each partition, it is to be noted that both the $\boldsymbol{G_1}$ and $\boldsymbol{G_2}$ matrix factors are evaluated using the same frequency as that indicated for the $\boldsymbol{G_2}$ matrices.

Representative Applications of the Methodology

Linear Systems

Application of the frequency-domain methodology to strictly linear systems is quite straightforward in that the component mobilities can be calculated directly without numerical integration of differential equations to obtain the frequency response functions. The results presented in Figs. 3a,b&c reflect the application of the methodology to a strictly linear system. The new methodology has significant practicality from the standpoint that the frequency response functions resulting from (linear) finite element modeling or shake-tests could be used directly and would not have to be converted to equivalent mass, damping and stiffness matrices.

For purposes of demonstrating the practicality of the frequency-domain methodology, two archived publications were used. The work of Tang and Dowell (Ref 8) was selected because it provides experimental results for a configuration with nonlinearities. The work of Hammond (Ref. 9) was selected because it provides results for a configuration with one lead-lag damper inoperative. It thus could be used as a touchstone for accurately duplicating the Floquet Theory calculations and thereby for validating the ground resonance calculations generally.

Application to Nonlinearities

The use of the new methodology to examine ground resonance instability characteristics of configurations with nonlinearities represents a straightforward computation. For present purposes, nonlinearities can be classified according to whether or not the nonlinearities are dominant at "small" amplitudes or only as the responses become large. In other words, is the configuration basically linear for the "small" displacements typical of incipient instability? For those cases wherein the system is nonlinear only for "large" responses, the determination of stability using the new methodology would give the same stability information for any selection of test force values that is reasonably "small" when calculating the frequency response function time-histories. The investigation of the limit-cycle characteristics associated with the nonlinearities is outwardly straightforward. All that is required is to vary the vibratory test force amplitudes until the system achieves the neutral stability condition, (i.e., unit values for Λ^*).

This is the approach followed herein for using the available experimental nonlinear ground resonance data. However, it should be kept in mind that the investigation of limit cycle conditions inherently involves macroscopic, i.e., "large" responses rather than infinitesimal ones. Thus, for consistency, the equations of motion must then address any nonlinearity resulting from the assumption of macroscopic responses.

The data from the experimental ground resonance model research performed by Tang and Dowell (Ref 8) were used to demonstrate the utility of the methodology in addressing conditions with nonlinearities. The data were obtained with a mechanical model originally designed to provide approximations to the separate dynamics of an

elastically connected fuselage and shaft (with attached rotor). These features are shown in Fig. 4:

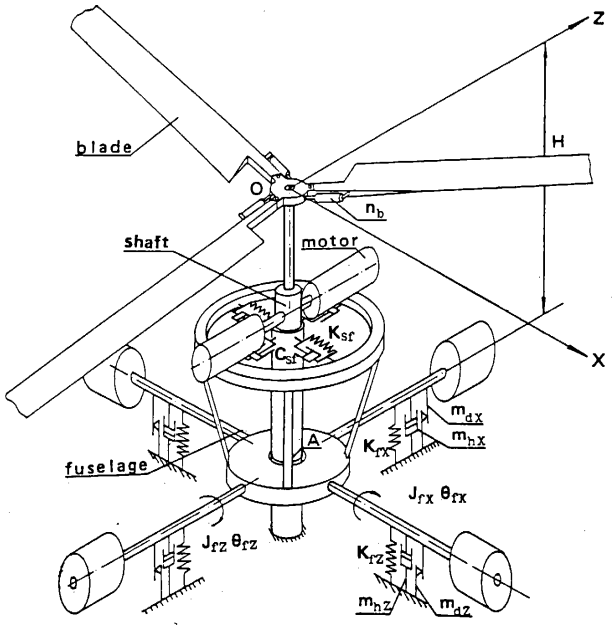

Fig. 4 Schematic of experimental apparatus (Tang & Dowell, Ref. 8)

The basic model system parameters, as gleaned from Ref. 8 and dimensionalized, are presented in Table 1. The "fuselage" parameters have been reduced to equivalent x-direction parameters. The given damping coefficient, C_{xF}, represents the residual linear damping exclusive of that provided by the discrete nonlinear dampers. The use of these data was compromised to a certain extent in that some of the pertinent data were not directly available.

Table 1 System parameters for the Tang & Dowell model (Ref. 8)

Rotor blade parameters:

m_b	=	0.01158 lb-sec^2/ft
S_b	=	0.0076 lb-sec^2
I_b	=	0.008108 lb-ft-sec^2
C_b	=	0.00425 lb-sec-ft
e	=	0.2083 ft.
R	=	1.5 ft
c	=	0.2083 ft.
n	=	3

Fuselage + shaft pitch (x-direction) parameters:

M_{xF}	=	0.3944 lb-sec^2/ft
C_{xF}	=	0.0248 lb-sec/ft
K_{xF}	=	16.517 lb/ft
H	=	1.520 ft

However, with some reasonable engineering assumptions the data were put in a form for use with the new methodology.

The model was provided with nonlinearities in the form of hydraulic dampers and dry-friction dampers, whose measured characteristics are respectively presented in Figures 5 and 6. Of the various cases examined by Tang and Dowell, only the "A" model, variation 1 (with only the (2) hydraulic dampers operating), and variation 2 (with both the (2) hydraulic and (2) dry-friction dampers operating), were addressed. The "A" model was defined as having the "shaft" and "fuselage" components ganged together with the "roll" motion locked out.

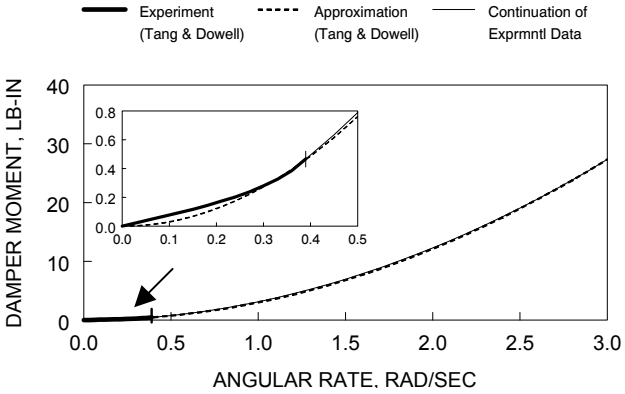

Fig. 5 Fixed system hydraulic damper characteristics

Difficulties were experienced with the system parameter data regarding the modeling of the dampers. Since the frequency-domain methodology uses integrations of the nonlinear equations (to obtain the *FRF*s), the complete empirically defined nonlinearities can be used directly. No idealizing to simple analytic functions is required.

The empirical descriptions of the damping characteristics were entered into the equation descriptions using cubic spline interpolations. Since some of the rates of motion experienced by the model were considerably in excess of the range originally given in Ref. 8, some extrapolation of the given experimental data was required. The cubic spline interpolation method automatically extends the data beyond the given range using the "end" slope (i.e, the first derivative calculated for the end point). Thus, one possible extrapolation scheme would be to use the results of the spline fit directly. Alternatively, a second extrapolation scheme, and the one used herein, was to continue the experimental data with a curve continuous with the end of the experimental data, but matching the Ref 8 idealization at an arbitrarily selected high pitch rate. Since the idealized hydraulic damping was given as: $M_{HD} = 3.04\ (d\theta/dt)\,|\,d\theta/dt\,|$, the "match" continuation was selected to duplicate the idealized value of M_{HD}

at a pitch rate of 3 rad/s. Thus, the continuation function (a quadratic function also) was set to give 27.36 lb-in at a pitch rate of 3 rad/s and then to maintain that "saturation" level for all pitch rates greater than 3 rad/s.

With regard to the dry friction damping, the idealization presented in Ref. 8 uses a constant value whose sign is determined by the sign of the angular rate: $M_{DF} = 0.054\ sgn(d\theta/dt)$. For the present study the measured characteristics were also used directly and continued at a constant value equal to the end value. The dry friction damping characteristics from Ref. 8 and those used herein are graphically defined in Fig. 6:

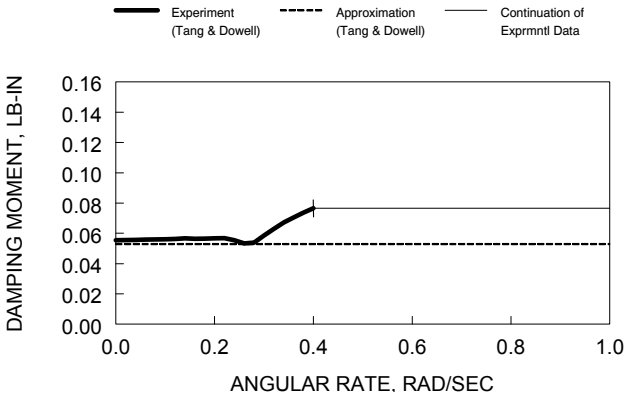

Fig. 6 Fixed system dry friction damper characteristics

It should be noted that a rigorous modeling of dry friction damping should probably include hysteretic effects, which could have easily have been included in the mathematical modeling, if the functionality were in fact known.

The second difficulty with damping parameters was with regard to the blade lead-lag damping. Simple quasi-steady aerodynamics shows that the aerodynamic damping available at rotor speed is of the same order-of-magnitude as the mechanical damping value given in Ref. 8. Furthermore, since the mechanical lead-lag dampers on the model are known to be of a primitive design (Ref. 10), it is unlikely that the damping is even linear or equal, at rotor speed, to any value that was determined by simple log decrement tests at zero rotor speed. The blade lead-lag damping was therefore varied and set at a value where the experimental results at the peak value could be duplicated, and then maintained at that value for the remainder of the study.

Results for Model A, Variation 1, Model with Only Hydraulic Dampers Since the hydraulic dampers are indeed nonlinear, the frequency response characteristics of the fuselage/shaft subsystem will be variable with the amplitude of the excitation force. The resulting *FRF* results for variation in excitation force amplitude are given in Fig. 7:

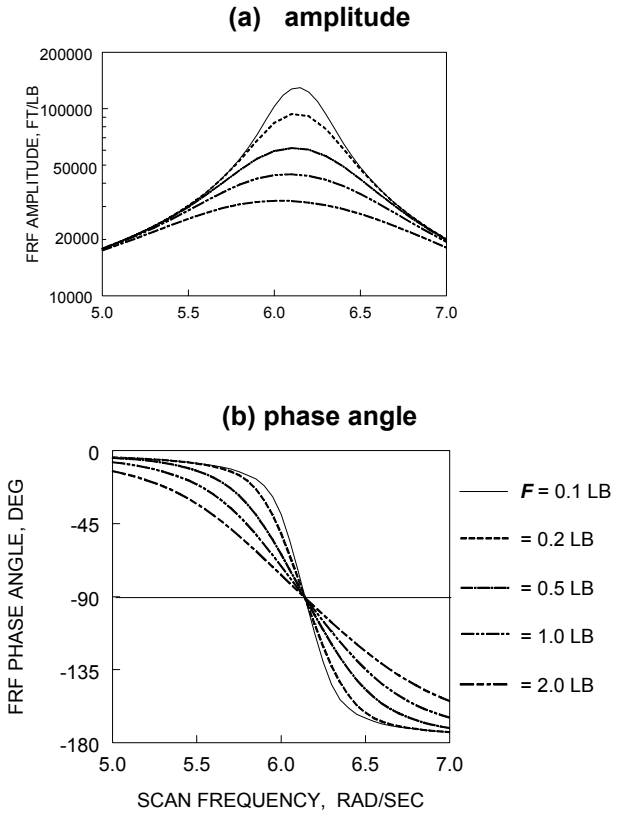

Fig. 7 Frequency response characteristics of the A Model with the hydraulic damper

The results of applying the frequency-domain methodology to the model in the A-1 configuration are presented in Fig. 8:

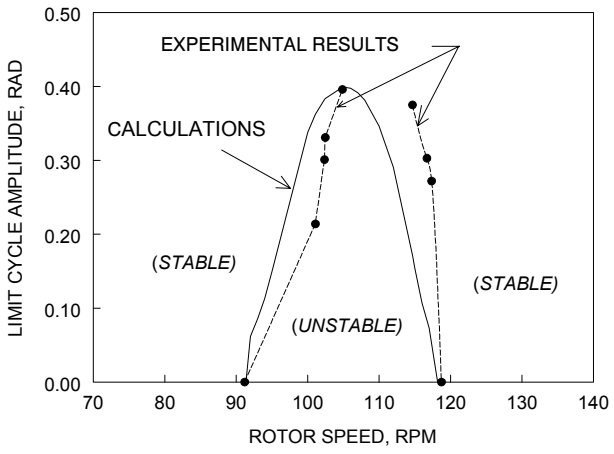

Fig. 8 Fuselage pitch limit cycle amplitude vs. rotor speed: A-model with hydraulic nonlinear damper only

The figure shows that the prediction of the basic stability boundary for incipient motion, i.e., where the

limit cycle approaches zero, is in excellent agreement with the experimental data. Of lesser importance is that much of the limit cycle character was also duplicated, with the rotor speed for maximum amplitude displaced from that found with the experimental results.

Results for Model A, Variation 2, Model with both Hydraulic and Dry-Friction Dampers The results of applying the frequency-domain methodology to the case where there are both types of nonlinear damping are shown in Fig. 9:

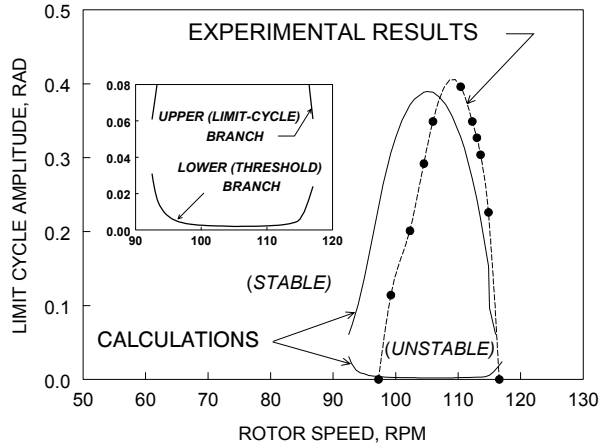

Fig. 9 Fuselage pitch limit cycle amplitude vs. rotor speed: A-model with both hydraulic and dry friction nonlinear dampers

Here the new methodology actually predicts two limit cycle boundaries: the obvious upper (limit cycle) branch, and a lower (threshold) branch with stable operation above the upper limit cycle branch and below the lower threshold branch. An explanation of this "threshold" behavior can be seen from the linearized (equivalent) damping coefficient for the dry friction model, C_E, using equivalent work per cycle (W_D) considerations:

$$W_D = C_E \theta^2 \omega \pi = 4 A_{DF} \theta \quad \rightarrow \quad C_E = \frac{4 A_{DF}}{\theta \omega \pi} \qquad (12)$$

where A_{DF} is the magnitude of the dry friction moment (≈ 0.054). Using Eq. 12, the results presented in Fig. 9 can be meaningfully interpreted. At small amplitudes, the equivalent damping from dry friction would thus be expected to predominate, and at large amplitudes the hydraulic damping should predominate. Fig. 9 shows that the peak limit cycle conditions for the A-1 and A-2 variations are essentially identical. The frequency-domain methodology predictions are seen to capture the reduced higher rotor speed boundary quite well. The lower rotor speed boundary is not so well predicted, however.

Real World Considerations

The limit cycle calculations presented in Figs. 8 and 9 are not intended to show actual correlation with the experimental data, but rather to show that the methodology can actually address the nonlinearities. A number of "real world" considerations can be identified and should be kept in mind in interpreting these results. First, the peak limit cycle results are heavily dependent on the damping characteristics of the nonlinear fuselage dampers at the high pitch rates, where the characteristics are only assumed. Likewise, the assumptions of linearity and effective damping coefficient for the lead-lag dampers are both suspect. Lastly, and perhaps most importantly, the usual linearized *infinitesimal amplitude* version of the blade equations was used in both the present study and in Ref. 8. An indication of the possible error engendered by this assumption is afforded by considering the blade lead-lag response amplitude at the maximum limit cycle conditions (i.e., rotor speed of 105 RPM, limit cycle amplitude of 0.4 radians and an oscillation frequency of 6.124 rad/sec). Using Eq. 4b, the blade inplane responses can be calculated from the fuselage motion:

$$\{X_R\} = \begin{Bmatrix} \varepsilon_x \\ \varepsilon_y \end{Bmatrix} = -[H_{22}]^{-1}[H_{21}]\{X_{F+R}\} \qquad (13)$$

$$= -\begin{bmatrix} I_b(\omega_e^2 - \Omega^2 - \omega^2) + i\omega C_b & \Omega(2i\omega I_b + C_b) \\ -\Omega(2i\omega I_b + C_b) & I_b(\omega_e^2 - \Omega^2 - \omega^2) + i\omega C_b \end{bmatrix}^{-1} \begin{Bmatrix} -\omega^2 S_b \\ 0 \end{Bmatrix} X_{HUB}$$

where the fore and aft displacement, X_{HUB}, is equal to $1.519 \times \theta$. For the selected maximum limit cycle condition this equation gives a lead-lag amplitude of 4.218 radians, or approximately 242 deg.! Clearly, a more exact math modeling would be required to predict the limit cycle conditions accurately.

Application to Dissimilar Blades (Double Anisotropy)

Fig. 10 presents the mathematical representation of the rotor and hub, as used in the Ref. 9 Hammond study. [This representation is perhaps the most basic modeling that can be used for ground resonance analyses]:

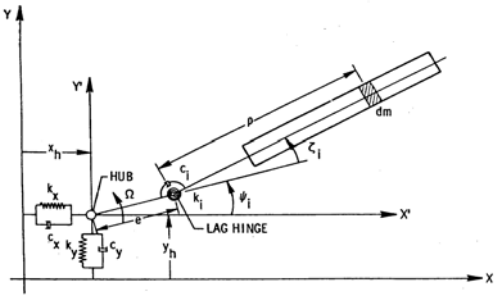

Fig. 10 Mathematical representation of the rotor and hub (Hammond, Ref 9)

The parameters used in the Hammond work are presented in Table 2. These parameters were selected "…so as to be in the general range of interest for a single rotor helicopter and were such that the system was stable with all dampers functioning up to a rotor speed of 400 rpm." The study investigated the stability characteristics of the selected configuration with two fuselage variants: isotropic, with both the x- and y- properties taken to be those given for the x-direction, and anisotropic, with all the values, as given in Table 2. The analytical results presented were all "exact" in that, for the isotropic (fuselage) case, the rotating coordinate system version of the equations, resulting in a constant coefficient matrix equation, was used. For the doubly anisotropic case (anisotropic fuselage and anisotropic rotor), the equations were written in the non-rotating coordinate system resulting in an eigenvalue problem with periodic coefficients. This case was solved with a standard application of Floquet Theory.

Table 2 System parameters used in the Hammond calculations (Ref 9)

Rotor blade parameters:	
m_b	= 6.5 lb-sec^2/ft
S_b	= 65.0 lb-sec^2
I_b	= 800.0 lb-ft-sec^2
C_b	= 3000.0 lb-sec-ft
e	= 1.0 ft.
n	= 4
Fuselage parameters:	
M_{xF}	= 550.0 lb-sec^2/ft
M_{yF}	= 225.0 lb-sec^2/ft
C_{xF}	= 3500.0 lb-sec/ft
C_{yF}	= 1750.0 lb-sec/ft
K_{xF}	= 85000.0 lb/ft
K_{yF}	= 85000.0 lb/ft

The Damper Effectivity Parameter In addition to the mathematical techniques required by Eqs. 9, 10, & 11, as well as the formulations in Appendix B, another consideration needs to be addressed. When one blade has an inactive lead-lag damper, the equations see an undamped subsystem, which causes the calculation of the requisite *FRF*'s to assume extremely large values. This in turn results in extremely large predictions of the characteristic multipliers. Consequently, the calculation of the real-axis crossings becomes subject to round-off errors. Real-world considerations, however, dictate that no elasto-mechanical system can have exactly zero damping. Indeed, even with a failed lead-lag damper the rotor blade will still experience some friction about the lead-lag hinge, as well as a finite amount of aero-dynamic damping due to drag. Thus, a justification for including a small amount of damping is justified. To this end, a damper effectivity parameter, K_e, is introduced, as a factor multiplying the standard amount of lead-lag damping (as given in Table 2).

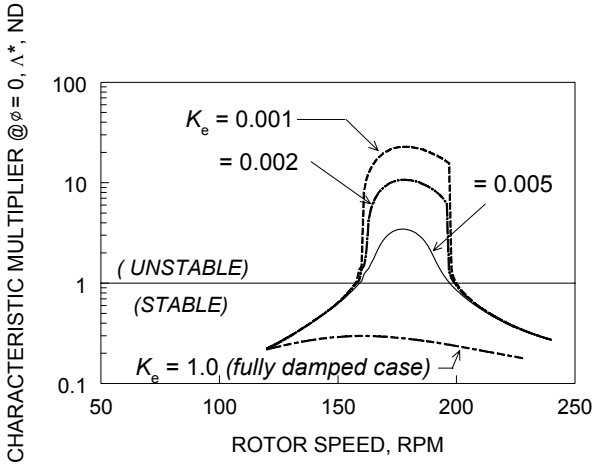

Fig. 11 Critial characteristic multipler variations with rotor speed and lead-lag effectivity - isotropic hub case, one lead-lag damper inoperative

Fig. 11 presents the calculated critical characteristic multiplier results for the isotropic fuselage wherein the rotor speed is varied as well as a limited variation on the damper effectivity parameter. The figure shows that, indeed, with full effectiveness on the one damper, the helicopter is stable, as expected. For small values of the parameter, however, large variations in the maximum values of the critical characteristic multiplier are experienced. However, for the critical points defining the stability boundaries (i.e., $\Lambda^* = 1$), there is little difference between the curves. Consequently, the 0.005 parameter value (i.e., 0.5% effectiveness) was selected because the resulting locus maintained a more or less constant order of magnitude. This value was then maintained for the remainder of the study.

The Isotropic Fuselage Case Fig. 12 presents the comparative results between the Ref. 13 results (as accurately reproduced using the rotating coordinate system formulation) and those predicted by the frequency-domain methodology. In order to compare the eigenvalue results with characteristic multiplier results the eigenvalue results were converted to "equivalent" characteristic multipliers by the expedient of exponentiating the real parts of the eigenvalues. This operation enables the stability boundaries predicted by both methodologies to be readily compared. A second variant, wherein a factor of ten was applied to the real part of the eigenvalue, was also used to accentuate the comparison. The results clearly show the excellent correlation between

the two methods for determining the stability boundaries.

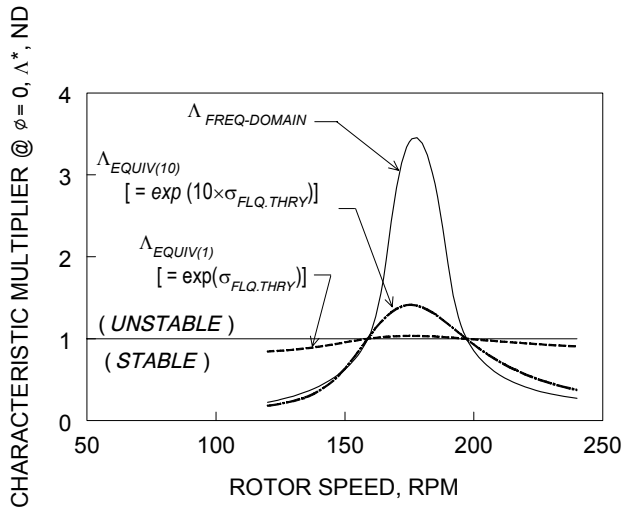

Fig. 12 Critical characteristic multiplier comparison – isotropic fuselage case, one lead-lag damper inactive, (K_e = 0.005)

To provide an alternate way of showing correlation, the characteristic multipliers were then converted to effective modal damping exponents, for comparison with those resulting from the eigenvalue calculations. The results of this comparison are shown in Fig. 13. For this purpose the logarithmic variants of the formulations in Appendix A were used.

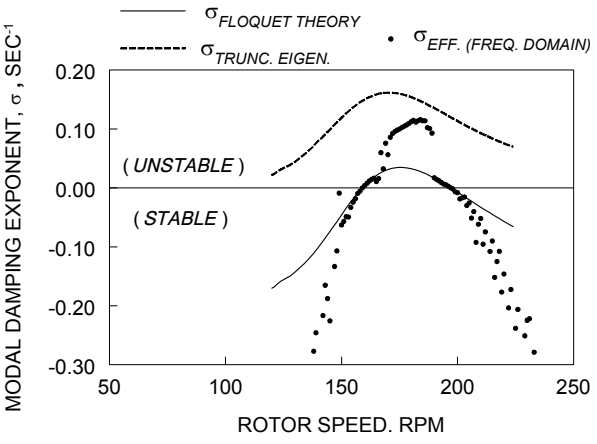

Fig. 13 Equivalent modal damping exponent comparison – isotropic fuselage case, one lead-lag damper inactive, (K_e = 0.005)

Also included in this figure are the exponents resulting from an application of an eigenvalue analysis of the equations with all the final harmonic terms neglected, i.e., truncated. The figure shows that with regard to the frequency-domain predictions, despite erratic excursions for most of the curve, those points close to the stability boundaries show excellent agreement with those from the exact eigenvalue analysis. The truncated eigenvalue analysis approach, however, is clearly too inaccurate to use.

The Anisotropic Fuselage Case When the fully anisotropic fuselage is considered, the distinction is essentially transparent to the frequency-domain methodology. Consequently, as shown in Fig. 14, the comparison of the stability boundaries predicted by the two methodologies is still excellent.

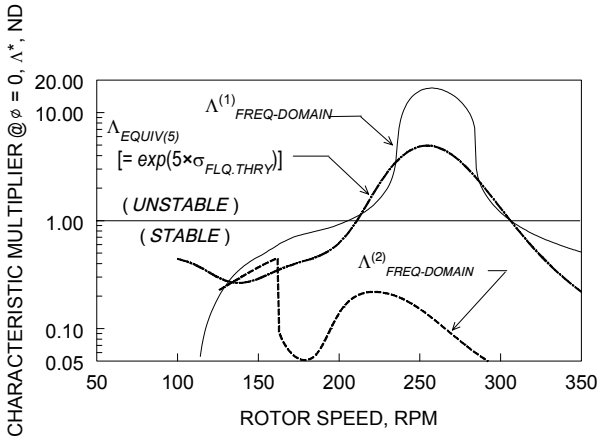

Fig. 14 Equivalent critical characteristic multiplier comparison – anisotropic fuselage case, one lead-lag damper inactive, (K_e = 0.005)

Note that for this case there is a second nontrivial characteristic multiplier present, but that characteristic multiplier remains always less than unity and, therefore, does not impact on the stability of the configuration.

Conclusions

The frequency-domain methodology described herein represents no less than a new paradigm for analyzing helicopter ground resonance. The methodology is seen to be a practical and accurate method for investigating not only simple (linear) configurations, but also addressing those with significant nonlinearities as well as the doubly anisotropic conditions associated with one lead-lag damper inoperative. By dividing the ground resonance problem into separate dynamic subsystems and treating them in the frequency domain, several problems associated with accurate test verification and the general treatments of a wide class of nonlinearities, are rectified. Specific conclusions are:

1. The stability boundaries predicted by the new methodology are determined by the loci of newly defined, frequency-dependent characteristic multi-

pliers exceeding the value of +1.0 when they cross the real axis. These stability boundaries are consistent with those predicted by traditional methods, i.e., matrix eigenvalue solutions and Floquet Theory.

2. Full-scale tests for verification of analysis can be safely performed in the frequency domain without the need for ascertaining effective mass, damping and stiffness matrices, and/or conducting inherently dangerous actual full scale tests for unstable behavior.

3. The analysis of the doubly anisotropic problem of a failed lead-lag damper requires frequency response data in three separate, but related frequency ranges.

4. The prediction of limit cycle conditions requires a careful attention to all the details of the nonlinearities, including the additional dynamic effects resulting from macroscopic responses.

5. The matrix eigenvalue problem defining the characteristic multipliers must be supplemented with additional processing algorithms for establishing appropriate sweep frequency ranges and determining the critical values of the characteristic multipliers.

It is to be noted that the use of the frequency-domain methodology should not completely obviate the use of the traditional eigenvalue methods. These methods can supplement the new methodology by providing information about the appropriate scan frequency range as well as providing sanity checks on the results. On a final note, it is to be appreciated that the basic stability boundary methodology developed herein is general enough that it can be applied to a broad range of other rotorcraft-related instability phenomena besides just ground resonance.

References

[1]Meirovitch, L., *Dynamics and Control of Structures*, John Wiley & Sons, New York, 1990.

[2]Bielawa, R. L., "An Improved Technique for Testing Helicopter Rotor-Pylon Aeromechanical Stability Using Measured Rotor Dynamic Impedance Characteristics,' *Vertica*, Vol. 9, No. 2, 1985, pp.181-197.

[3]Coleman, R. P. & Feingold, A. M., "Theory of Self-Excited Mechanical Oscillations of Helicopter Rotors with Hinged Blades,' *NACA Report 1351*, 1958.

[4]Bielawa, R. L., *Rotary Wing Structural Dynamics and Aeroelasticity*, R. L. Bielawa, AIAA Education Series, Washington D.C., 1992.

[5]Ralston,A., & Wilf, *Mathematical Methods for Digital Computers*, John Wiley and Sons, New York, 1960.

[6]Savant, C. J., *Basic Feedback Control System Design*, McGraw-Hill Book Company, New York, 1958.

[7]Press, W.H., Flannery, B. P., Teukolsky, S. A., & Vetterling, W. T., Numerical Recipes, Cambridge University Press, New York, 1988.

[8]Tang, D. M. & Dowell, E. H., "Effects of Nonlinear Damping in Landing Gear on Helicopter Limit Cycle Response in Ground Resonance," Journal of the American Helicopter Society, Vol. 32, No. 1, pp. 45-53.

[9]Hammond, C. E., "An Application of Floquet Theory Prediction of Mechanical Instability," AHS/NASA Ames Specialists' Meeting on Rotorcraft Dynamics, NASA Ames Research Ctr., Feb. 1974.

[10] Bielawa, R. L., "An Experimental and Analytical Study of the Mechanical Instability of Rotors on Multiple-Degree-of-Freedom Supports," Department of Aeronautical Engineering Report no. 612, Princeton University, June 1962.

Appendix A – Effective Damping Exponents

Essentially, the objective here is to recoup, at least approximately, the eigenvalue results (i.e., $\lambda = \sigma \pm i\omega$) from the characteristic multiplier results (i.e., $\Lambda = \Lambda_R \pm i\Lambda_I$). In a typical application of this methodology the characteristic multiplier stability information would be available only as numerical values of magnitude and phase of Λ for a few frequencies near the positive real-axis crossing. Numerical techniques can be used to obtain the actual real-axis crossing values of ω and Λ. However, in order to recoup, at least approximately, the equivalent eigenvalue (characteristic exponent) results, a straightforward application of analytic continuation can be performed about the point $\Lambda = 1 + \varepsilon + i0$. This formulation begins by writing Eq. 1 in the following more general form:

$$\Lambda(\lambda_1)\{X\} - [G_1(\lambda_1)][G_2(\lambda_1)]\{X\} = \{0\} \quad \text{(A.1)}$$

where, for the usual eigenvalue solution, $\lambda_1 = \lambda = \sigma \pm i\omega$, and $\Lambda(\lambda_1) = +1$. However, the characteristic multiplier solution is known only for λ on the imaginary axis: $\lambda_1 = i\omega$, and $\Lambda(\lambda_1) = \Lambda_R + i\Lambda_I$. The objective is to closely approximate the characteristic exponent σ knowing the behavior of Λ as a function of ω near the critical point. Note first that, in the frequency domain as noted earlier, $\Lambda(i\omega)$, will have the value of $1 + \varepsilon$ (where ε is a calculable, but reasonably "small" quantity only near the stability boundary), at the real axis crossing frequency, $\omega = \omega^*$ (also known). In the Laplace-variable domain, however, $\Lambda(\lambda)$ has the value of exactly 1 at the value of λ that we seek. Assuming that $\Lambda(\lambda)$ is

an analytic function in the neighborhood of (1 + i 0), we can, therefore, expand $\Lambda(\lambda)$ in a Taylor Series taking the derivatives in the frequency (imaginary) axis direction and evaluating them at the point $\lambda = \lambda^* = i\,\omega^*$, where ω^* is the frequency at the real-axis crossing. At the real-axis crossing point, we represent the characteristic multiplier $\Lambda(\lambda^*)$ as (1 + ε). The analytic continuation equation then becomes:

$$\Lambda(\lambda) = 1 = 1 + \varepsilon + (\lambda - \lambda^*)\frac{d\Lambda}{d\lambda}(\lambda^*) + \frac{1}{2}(\lambda - \lambda^*)^2 \frac{d^2\Lambda}{d\lambda^2}(\lambda^*) + \ldots \tag{A.2}$$

We note that:

$$\frac{d\Lambda}{d\lambda} = \frac{d\Lambda_R}{d(i\omega)} + i\frac{d\Lambda_I}{d(i\omega)} = \frac{d\Lambda_I}{d\omega} - i\frac{d\Lambda_R}{d\omega} \tag{A.3a}$$

$$\frac{d^2\Lambda}{d\lambda^2} = \frac{d}{d(i\omega)}\left(\frac{d\Lambda}{d(i\omega)}\right) = -\frac{d^2\Lambda_R}{d\omega^2} - i\frac{d^2\Lambda_I}{d\omega^2} \tag{A.3b}$$

and:

$$(\lambda - \lambda^*) \equiv \sigma + \boldsymbol{i}\Delta\omega \tag{A.4}$$

where: $\Delta\omega = \omega - \omega^*$. Since $\Lambda(\omega)$ would be known numerically only at a few distinct points (corresponding to discrete values of ω) near the (1 + ε + i0) point in the complex plane, a numerical curve fit calculation must be made to evaluate the derivatives. One efficient method of fitting the points to analytic approximations to the real and imaginary parts of $\Lambda(\omega)$ is the use of cubic spline interpolation. Since spline fit interpolation schemes fit the data points, as well as the second derivatives, they also provide an excellent method for approximating first and second derivatives. Thus, the use of cubic spline fits would limit the ability to extend Eq. A.2 beyond the second derivative term. The most accurate estimate of the damping and frequency, σ and ω, would thus entail only retaining the second-order derivative term in Eq. A.2:

$$\frac{1}{2}\frac{d^2\Lambda}{d(i\omega)^2}(\lambda - \lambda^*)^2 + \frac{d\Lambda}{d(i\omega)}(\lambda - \lambda^*) + \varepsilon \cong 0 \tag{A.5}$$

Solution of Eq. A.5 is perhaps most practically accomplished using the binomial theorem with complex arithmetic. It is to be expected that the accuracy of Eq. A.5 to give an analytic continuation would be most accurate only when ε is small (i.e., Λ is close to 1 + i 0). For cases where the zero-phase crossing is at a value significantly greater than unity, the use of the inverse of Λ is more useful. In this case the analytic continuation occurs about the point Λ^{-1} ($i\omega^*$), where:

$$\Lambda^{-1}(i\omega^*) = 1 - \hat{\varepsilon}\,; \quad \hat{\varepsilon} = \frac{\varepsilon}{1+\varepsilon} \tag{A.6}$$

The appropriate equation for solving for (λ - λ^*) using the inverse of Λ, then becomes:

$$\frac{1}{2}\frac{d^2(\Lambda^{-1})}{d(i\omega)^2}(\lambda - \lambda^*)^2 + \frac{d(\Lambda^{-1})}{d(i\omega)}(\lambda - \lambda^*) - \hat{\varepsilon} \cong 0 \tag{A.7}$$

Eq. A.7 is quite useful in that, for any unstable characteristic multiplier (i.e., $\Lambda^* = 1 + \varepsilon$), the deviation of $\Lambda^{-1}(i\omega^*)$ from unity is always less than 1., thereby affording a more accurate analytic continuation. Consequently, Eq. A.5 would more appropriately be used for stable characteristic multipliers and Eq. A.7 for the unstable ones.

Another variant of the analytic continuation scheme is to use the function *ln*(Λ). The appropriate quadratic equation then becomes:

$$\frac{1}{2}\frac{d^2(\ln(\Lambda))}{d(i\omega)^2}(\lambda - \lambda^*)^2 + \frac{d(\ln(\Lambda))}{d(i\omega)}(\lambda - \lambda^*) + \breve{\varepsilon} \cong 0 \tag{A.8}$$

where:

$$\frac{d(\ln\Lambda)}{d(i\omega)} = \frac{1}{\Lambda}\frac{d\Lambda}{d(i\omega)} = \Lambda^{-1}\frac{d\Lambda}{d(i\omega)}\,; \tag{A.9a}$$

$$\frac{d^2(\ln\Lambda)}{d(i\omega)^2} = \Lambda^{-1}\frac{d^2\Lambda}{d(i\omega)^2} + \frac{d(\Lambda^{-1})}{d(i\omega)}\frac{d\Lambda}{d(i\omega)} \tag{A.9b}$$

and:

$$\breve{\varepsilon} = \ln\Lambda^* \tag{A.10}$$

In a similar manner *ln*(Λ^{-1}) can be used:

$$\frac{1}{2}\frac{d^2(\ln(\Lambda^{-1}))}{d(i\omega)^2}(\lambda - \lambda^*)^2 + \frac{d(\ln(\Lambda^{-1}))}{d(i\omega)}(\lambda - \lambda^*) - \breve{\varepsilon} \cong 0 \tag{A.11}$$

where:

$$\frac{d(\ln\Lambda^{-1})}{d(i\omega)} = \Lambda\frac{d(\Lambda^{-1})}{d(i\omega)}\,; \tag{A.12a}$$

$$\frac{d^2(\ln\Lambda^{-1})}{d(i\omega)^2} = \Lambda\frac{d^2(\Lambda^{-1})}{d(i\omega)^2} + \frac{d(\Lambda^{-1})}{d(i\omega)}\frac{d\Lambda}{d(i\omega)} \tag{A.12b}$$

Appendix B - Extension of Methodology to the One Dissimilar Blade Case

The following development is directly applicable to the four-bladed rotor, and can be extended to any even-number bladed rotor. Following the synopsis given in the body of this paper, we first represent the blade lead-lag motions, $\varepsilon^{(i)}$, with a generalization of the usual rotor mode (multi-blade) coordinate set:

$$\varepsilon^{(i)} = \varepsilon_y^{(i)}\cos\left(\Omega t + \frac{2\pi\, m^{(i)}}{b}\right) - \varepsilon_x^{(i)}\sin\left(\Omega t + \frac{2\pi\, m^{(i)}}{b}\right) \tag{B.1}$$

where:

i = 1: the two opposing undifferentiated blades (blade nos. 1 & 3, $m^{(1)} = 0$)

= 2: the one dissimilar blade, (blade no. 2, $m^{(2)} = \pi/2$)

= 3: the remaining undifferentiated blade, opposing the dissimilar blade (blade no. 4, $m^{(4)} = 3\pi/2$)

Blade equations: The three sets of blade equation pairs can all be represented by the following equations:

$$I_b\left\{\ddot{\varepsilon}_x^{(i)} + \eta_i\dot{\varepsilon}_x^{(i)} + (\omega_\varepsilon^2 - \Omega^2)\varepsilon_x^{(i)} + 2\Omega\left(\dot{\varepsilon}_y^{(i)} + \eta_i\varepsilon_y^{(i)}\right)\right\} + S_b\ddot{x} = 0 \quad \text{(B.2a)}$$

$$I_b\left\{\ddot{\varepsilon}_y^{(i)} + \eta_i\dot{\varepsilon}_y^{(i)} + (\omega_\varepsilon^2 - \Omega^2)\varepsilon_y^{(i)} - 2\Omega\left(\dot{\varepsilon}_x^{(i)} + \eta_i\varepsilon_x^{(i)}\right)\right\} + S_b\ddot{y} = 0 \quad \text{(B.2b)}$$

where: η_i is equal to the undifferentiated blade lead-lag damping coefficient for i = 1 & 3 and to the dissimilar damping coefficient (i.e., the undifferentiated value $\times$ K_e) for i = 2. Thus, Eqs. B.2a&b actually represent six dynamic equations (three pairs of coupled equations).

Fuselage equations: The dynamic equations governing the x- and y- fuselage hub motion are straightforward extensions of the usual equations for hub motion, except there are now explicit contributions from the three lead-lag configurations:

longitudinal (x-direction) motion:

$$\begin{aligned} &M_{xF}\ddot{x} + C_{xF}\dot{x} + K_{xF}x + \\ &\frac{S_b}{2}\left\{2\left[\ddot{\varepsilon}_x^{(1)} + \left(\ddot{\varepsilon}_x^{(1)} + 4\Omega\dot{\varepsilon}_y^{(1)} - 4\Omega^2\varepsilon_x^{(1)}\right)\cos 2\Omega t\right.\right. \\ &\qquad \left.\left. + \left(\ddot{\varepsilon}_y^{(1)} - 4\Omega\dot{\varepsilon}_x^{(1)} - 4\Omega^2\varepsilon_y^{(1)}\right)\sin 2\Omega t\right] \\ &\quad + \ddot{\varepsilon}_x^{(2)} - \left(\ddot{\varepsilon}_x^{(2)} + 4\Omega\dot{\varepsilon}_y^{(2)} - 4\Omega^2\varepsilon_x^{(2)}\right)\cos 2\Omega t \\ &\qquad - \left(\ddot{\varepsilon}_y^{(2)} - 4\Omega\dot{\varepsilon}_x^{(2)} - 4\Omega^2\varepsilon_y^{(2)}\right)\sin 2\Omega t \\ &\quad + \ddot{\varepsilon}_x^{(3)} - \left(\ddot{\varepsilon}_x^{(3)} + 4\Omega\dot{\varepsilon}_y^{(3)} - 4\Omega^2\varepsilon_x^{(3)}\right)\cos 2\Omega t \\ &\qquad \left. - \left(\ddot{\varepsilon}_y^{(3)} - 4\Omega\dot{\varepsilon}_x^{(3)} - 4\Omega^2\varepsilon_y^{(3)}\right)\sin 2\Omega t\right\} = 0 \end{aligned} \quad \text{(B.3)}$$

lateral (y-direction) motion:

$$\begin{aligned} &M_{yF}\ddot{y} + C_{yF}\dot{y} + K_{yF}y + \\ &\frac{S_b}{2}\left\{2\left[\ddot{\varepsilon}_y^{(1)} - \left(\ddot{\varepsilon}_y^{(1)} - 4\Omega\dot{\varepsilon}_x^{(1)} - 4\Omega^2\varepsilon_y^{(1)}\right)\cos 2\Omega t\right.\right. \\ &\qquad \left.\left. + \left(\ddot{\varepsilon}_x^{(1)} + 4\Omega\dot{\varepsilon}_y^{(1)} - 4\Omega^2\varepsilon_x^{(1)}\right)\sin 2\Omega t\right] \\ &\quad + \ddot{\varepsilon}_y^{(2)} + \left(\ddot{\varepsilon}_y^{(2)} - 4\Omega\dot{\varepsilon}_x^{(2)} - 4\Omega^2\varepsilon_y^{(2)}\right)\cos 2\Omega t \\ &\qquad - \left(\ddot{\varepsilon}_x^{(2)} + 4\Omega\dot{\varepsilon}_y^{(2)} - 4\Omega^2\varepsilon_x^{(2)}\right)\sin 2\Omega t \\ &\quad + \ddot{\varepsilon}_y^{(3)} + \left(\ddot{\varepsilon}_y^{(3)} - 4\Omega\dot{\varepsilon}_x^{(3)} - 4\Omega^2\varepsilon_y^{(3)}\right)\cos 2\Omega t \\ &\qquad \left. - \left(\ddot{\varepsilon}_x^{(3)} + 4\Omega\dot{\varepsilon}_y^{(3)} - 4\Omega^2\varepsilon_x^{(3)}\right)\sin 2\Omega t\right\} = 0 \end{aligned} \quad \text{(B.4)}$$

Note that if $\varepsilon^{(1)} = \varepsilon^{(2)} = \varepsilon^{(3)} = \varepsilon$, the usual Coleman (i.e., constant coefficient) form of the dynamic equations results. Using the definitions for $\boldsymbol{G}_1(\omega)$ and $\boldsymbol{G}_2(\omega)$ given by Eqs. 13a&b, and assuming sinusoidal motion, one finds the various matrices to be as follows:

$$\begin{aligned} G_1(\omega) &= H_{11}^{-1} \\ &= \begin{bmatrix} \left(K_{xF} - M_{xF}\omega^2\right) + i\omega C_{xF} & 0 \\ 0 & \left[\left(K_{yF} - M_{yF}\omega^2\right) + i\omega C_{yF}\right] \end{bmatrix}^{-1} \end{aligned} \quad \text{(B.5)}$$

$$H_{21}(\omega) = -\frac{S_b}{2}\begin{bmatrix} 1 & 0 & 1 & 0 & 1 & 0 \\ 0 & 1 & 0 & 1 & 0 & 1 \end{bmatrix}^T \omega^2 \quad \text{(B.6)}$$

$$\begin{aligned} H_{12}(\omega) &= \frac{S_b}{2}\left[-\omega^2 U_1 + (-\omega^2 U_2 + 4i\omega U_3 + 4\Omega^2 U_2)\cos 2\Omega t\right. \\ &\qquad \left. + (-\omega^2 U_3 - 4i\omega U_2 + 4\Omega^2 U_3)\sin 2\Omega t\right] \\ &= \frac{S_b}{4}\left\langle -2\omega^2 U_1 + \left[-(\omega - 2\Omega)^2 U_2 - i(\omega + 2\Omega)^2 U_3\right]e^{2i\Omega t}\right. \\ &\qquad \left. - \left[(\omega + 2\Omega)^2 U_2 + i(\omega - 2\Omega)^2 U_3\right]e^{-2i\Omega t}\right\rangle \end{aligned} \quad \text{(B.7)}$$

where:

$$U_1 = \begin{bmatrix} 2 & 0 & 1 & 0 & 1 & 0 \\ 0 & 2 & 0 & 1 & 0 & 1 \end{bmatrix} \quad \text{(B.8a)}$$

$$U_2 = \begin{bmatrix} 2 & 0 & -1 & 0 & -1 & 0 \\ 0 & -2 & 0 & 1 & 0 & 1 \end{bmatrix} \quad \text{(B.8b)}$$

$$U_3 = \begin{bmatrix} 0 & 2 & 0 & -1 & 0 & -1 \\ 2 & 0 & -1 & 0 & -1 & 0 \end{bmatrix} \quad \text{(B.8c)}$$

Continuing:

$$H_{22}^{-1} = \begin{bmatrix} H_{22}^{(1)} & 0 & 0 \\ 0 & H_{22}^{(2)} & 0 \\ 0 & 0 & H_{22}^{(3)} \end{bmatrix}^{-1} \quad \text{(B.9a)}$$

where:

$$H_{22}^{(1)} = I_b\begin{bmatrix} \left[-(\omega^2 + \omega_e^2 + \Omega^2) + i\omega\eta_1\right] & 2\Omega(i\omega + \eta_1) \\ -2\Omega(i\omega + \eta_1) & \left[-(\omega^2 + \omega_e^2 + \Omega^2) + i\omega\eta_1\right] \end{bmatrix}$$

$$H_{22}^{(2)} = I_b\begin{bmatrix} \left[-(\omega^2 + \omega_e^2 + \Omega^2) + i\omega\eta_2\right] & 2\Omega(i\omega + \eta_2) \\ -2\Omega(i\omega + \eta_2) & \left[-(\omega^2 + \omega_e^2 + \Omega^2) + i\omega\eta_2\right] \end{bmatrix}$$

$$H_{22}^{(3)} = I_b\begin{bmatrix} \left[-(\omega^2 + \omega_e^2 + \Omega^2) + i\omega\eta_3\right] & 2\Omega(i\omega + \eta_3) \\ -2\Omega(i\omega + \eta_3) & \left[-(\omega^2 + \omega_e^2 + \Omega^2) + i\omega\eta_3\right] \end{bmatrix}$$

(B.9b,c,d)

Using Eqs. B.6 thru B.9, one can then easily compute the $\boldsymbol{G}_2(\omega)$ matrix (as defined by Eq. 10b).